

THE CYCLOTRON FUNDAMENTAL EXPOSED IN THE HIGH-FIELD MAGNETIC VARIABLE V884 HER

GARY D. SCHMIDT^{1,2}, LILIA FERRARIO², D. T. WICKRAMASINGHE², AND PAUL S. SMITH¹
To appear in The Astrophysical Journal, Part 1

ABSTRACT

High-quality phase-resolved optical spectropolarimetry is presented for the magnetic cataclysmic variable V884 Her. The overall circular polarization during active accretion states is low and only slightly variable in the range 5000 – 8000 Å. However, the polarization is highly structured with wavelength, showing very broad polarization humps, narrow features that are associated with weak absorption lines in the total spectral flux, and sharp reversals across each major emission line. The polarization reversals arise from Zeeman splitting in the funnel gas in a longitudinal magnetic field $B \sim 30$ kG. The set of narrow, polarized absorption features matches the Zeeman pattern of hydrogen for a nearly uniform magnetic field of $B = 150$ MG, indicating that the features are “halo” absorption lines formed in a relatively cool reversing layer above the shock. With this identification, the broad polarization humps centered near 7150 Å and below 4000 Å are assigned to cyclotron emission from the fundamental and first harmonic ($n = 2$), respectively. V884 Her is only the second AM Her system known with a field exceeding 100 MG, and the first case in which the cyclotron fundamental has been directly observed from a magnetic white dwarf.

Subject headings: stars: magnetic fields — stars: individual: V884 Her — cataclysmic variables — accretion — polarization

1. INTRODUCTION

The fate of cataclysmic variables containing the most highly magnetic primary stars has long been a mystery. Though single magnetic white dwarfs are distributed continuously up to nearly 10^9 G (e.g., Wickramasinghe & Ferrario 2000), some 3 dozen AM Her-type variables (“polars”) were measured to have polar field strengths $B_p < 80$ MG (MG = 10^6 G) before the first high-field example, AR UMa, was discovered at $B_p = 230$ MG (Schmidt et al. 1996). The observed characteristics of AR UMa raised suspicions that the high- B examples might violate some of the hallmarks of the class: A very large flux ratio of soft to hard X-rays suggests that the accreting gas penetrates deeply into the photosphere, avoiding a standoff shock (e.g., Stockman 1988). As a result, the optical circular polarization of AR UMa during an active accretion state is nearly nil (Schmidt et al. 1996). The magnetic white dwarf is also twisted in azimuth so that the magnetic axis is nearly orthogonal to the stellar line of centers. Finally, AR UMa has spent the majority of the past several years in a state of inactivity, with accretion episodes lasting at most a few months (Schmidt et al. 1999). The implication is that a successful quest for high- B cataclysmic variables (CVs) may require broadening our definition of what constitutes a magnetic accretion binary.

One clue in the search is the trend toward increasing soft X-ray “excess” with increasing magnetic field strength (Ramsay et al. 1994), apparently caused by the progressive reduction in shock height and burying of high-density portions of the accretion flow. The most extreme example in this regard is V884 Her (=RX J1802.1+1804), an optically bright ($m_V \sim 14 - 16$) but very low-polarization system ($v \lesssim 4\%$; Szkody et al. 1995) that has been found to

have a soft-to-hard X-ray flux ratio $F_{SX}/F_{HX} \sim 10^3 - 10^4$ (Greiner, Remillard, & Motch 1998; Ishida et al. 1998; Szkody et al. 1999). The orbital period of V884 Her is 113.01 min (1.8835 hr; Greiner et al. 1998) and characterized by periodic dips in the X-ray light curve whose depth shows strong energy dependence indicative of self-eclipse by the gas stream. Similar features are present in the EUV (Hastings et al. 1999), but the optical light curve is less well-behaved. There is no detection yet of either stellar component, a fact that prevents a reliable estimate of distance and of the orbital location of the secondary at the time of the X-ray dip. Some variation in accretion activity is implied by 1 – 2 mag changes in optical brightness with epoch, but thus far the binary has shown nothing resembling an “off” accretion state, and Hastings et al. (1999) conclude that high-state emission sources dominate even when $m_V \sim 16$. The system geometry is uncertain, but indications are of a rather low inclination ($i \sim 45^\circ$) and small magnetic colatitude ($\delta \sim 15^\circ$) with a short ballistic section to the accretion stream (Greiner et al. 1998; Hastings et al. 1999).

In this paper we present the results of phase-resolved optical spectrophotometry, polarimetry, and spectropolarimetry of V884 Her that reveal a circular polarization spectrum far more structured than any yet seen from a magnetic CV. Very broad polarization features are interpreted as emission in the cyclotron fundamental and first harmonic in a magnetic field $B \sim 115 - 130$ MG, while a number of narrow features in polarized flux are successfully modeled by hydrogen Zeeman features in a 150 MG accretion “halo” above the shock. V884 Her reveals an important and heretofore unobserved region of the spectrum of a magnetic accretion binary surrounding the cyclotron

¹Steward Observatory, The University of Arizona, Tucson, AZ 85721

²Dept. of Mathematics, The Australian National University, Canberra, ACT 0200 Australia

fundamental.

2. OBSERVATIONS AND RESULTS

The bulk of the data reported here was acquired with the CCD Spectropolarimeter (Schmidt, Stockman, & Smith 1992) operating on the Steward Observatory 2.3 m Bok telescope atop Kitt Peak. The instrument was configured for circular polarimetry over a full order of the grating, $\lambda\lambda 4000 - 8000$, providing a spectral resolution of $\sim 12 \text{ \AA}$. All or most of an orbital period was covered on each of 3 epochs during the period 1998 – 2000, with waveplate sequences limited to ~ 10 min in length to achieve phase resolution of $\Delta\varphi \leq 0.1$. The system brightness³ and degree of polarization from these measurements are summarized in Table 1, together with the range in orbital phase, computed from the X-ray dip ephemeris of Greiner et al. (1998):

$$\text{HJD} = 2449242.3124(21) + 0.07847977(11) E . \quad (1)$$

Additional single spectra were obtained as indicated in Table 1 to monitor the state of activity, and a full orbit of “white-light” ($\lambda\lambda 3200 - 8600$) linear polarimetry with phase resolution $\Delta\varphi = 0.025$ was obtained with a filter polarimeter and the Steward Observatory 1.5 m telescope on Mt. Lemmon. The latter data reveal no convincing detection of linear polarization above a 3σ uncertainty level of $P = 2\%$ for any sample during the series, such as might occur from the beaming pattern of high-harmonic cyclotron emission. Moreover, the orbit-averaged result is only marginally significant at $P = 0.30 \pm 0.11\%$; $\theta = 164^\circ \pm 11^\circ$. A brightness modulation of amplitude 0.35 mag is, however, apparent in the detected count rate at the 1.88 hr orbital period.

The various observing runs sampled somewhat different levels of system activity as indicated by the ~ 1 mag spread in the visual magnitudes in Table 1, but all of the spectropolarimetry show the same fundamental features: a strong emission-line spectrum superposed on a blue continuum that steepens in F_λ below 5000 Å and shows no sign of late-type stellar features at red wavelengths. Emission-line ratios are typical for an AM Her system in an active accretion state, with $F_{\text{H}\alpha} \approx F_{\text{H}\beta} \approx F_{\text{H}\gamma} \approx F_{\lambda 4686}$. The circular polarization is rather weak for a synchronized system, $|v| \lesssim 5\%$ over the region 5000 – 8000 Å. However, a very broad ($\Delta\lambda \sim 1000 \text{ \AA}$) negative polarization bump is centered near $\lambda 7300$ and negative polarization sets in also for $\lambda \lesssim 5700 \text{ \AA}$. The polarization increases sharply to generally positive values around $\lambda 4500$ and shows a great deal of structure. Finally, several “narrow” features, $\Delta\lambda \sim 100 \text{ \AA}$, are scattered through the spectrum. These basic characteristics are evident in the orbit-averaged results from 1999 Sep. 14 shown as Figure 1.

2.1. Time Dependence

Despite the differences in activity level, the spectrum-summed circular polarization is negative at all 3 epochs, as it was when observed by Szkody et al. (1995). Only a partial orbit was acquired on 2000 Mar. 10, yet the polarization in this brighter state appears only slightly reduced in absolute value. When the individual spectra are

phased according to the ephemeris in eq. (1), significant Doppler motion of the emission lines is apparent, reflecting the orbital modulation noted in previous spectroscopy. To study the polarization at the highest signal-to-noise ratio (S/N), this variation was removed from both the total flux and polarization spectra using a half-amplitude of 150 km s^{-1} (e.g., Greiner et al. 1998, Hastings et al. 1999), and the data from the multiple epochs were then coadded into phase bins. The results are shown in Figure 2 as a phase sequence of circularly polarized flux, $v \times F_\lambda$, and in Figure 3 as the phase dependence of circular polarization in broad spectral bands selected to isolate major polarization features. The grand sum is displayed together with the coadded spectral flux at an expanded scale in Figure 4.

It is evident from Figures 2 and 3 that the polarized emission for $\lambda \gtrsim 5000 \text{ \AA}$ is largely constant throughout the orbit. Variations are most apparent at the shortest wavelengths, where the polarized flux is strongly positive soon after $\varphi = 0$, switching to generally negative during the opposite half of the orbit. Several of the narrow polarization features noted above can be traced through the phase sequence in Figure 2, and, as is evident in Figure 4, those which are uncontaminated by line emission are accompanied by subtle depressions in the total flux. The facts that each of these absorption features exhibits a constant sign of polarization and shows very little movement in wavelength indicate that, if they are Zeeman in nature, only small changes in the mean magnetic field strength can occur through the orbit. We will find that this conclusion has important implications for the origin of the features.

2.2. A Magnetized Accretion Funnel

The circularly polarized flux displayed in Figure 2 and particularly in Figure 4 shows sharp polarization reversals across each major emission line. These are clear signatures of Zeeman splitting in the funnel gas. The reality of the features can be best appreciated from the individual panels of the coadded sum shown as Figure 5, where the *sense* of the reversals ($-$ for $\lambda < \lambda_0$, $+$ for $\lambda > \lambda_0$) is seen to be common for all, and the inflection in polarized flux occurs at line center for each transition. The quality of the phase-binned polarimetry in Figure 2 is sufficient to demonstrate that the sense of the splitting is also constant throughout the orbit, however any estimate of phase-dependent variation in the separation of the peaks would be severely limited by the spectral resolution and S/N of the data. We therefore measure the magnetic field present in the emission-line region from the coadded panels of Figure 5.

The separation of the opposing polarization peaks ranges from 15 Å for H δ to 20 Å for H α . In weak fields such as this, the Zeeman effect appears as a linear triplet for these transitions, and the σ components separate from the central π component at a rate of $\pm 20 \text{ \AA MG}^{-1}$ at H α , scaling as λ_0^2 . At face value this would suggest a magnetic field strength of $\sim 500 \text{ kG}$ ($\text{kG} = 10^3 \text{ G}$). However, this approach is invalid when the splitting is similar to the spectral resolution of the data, a conclusion verified by the fact that the field values so derived for the individual features increase monotonically from $\sim 400 \text{ kG}$ at H α

³These continuum magnitudes will register somewhat fainter than broadband measurements because of the presence of emission lines in the filter bands.

to nearly 800 kG for the shortest-wavelength lines. Moreover, this treatment ignores the fact that the emission line in total flux possesses wings out to $\sim 1500 \text{ km s}^{-1}$ ($\pm 25 \text{ \AA}$) from line center, and that the entire profile probably experiences the magnetic field. A proper approach must treat the line as two oppositely-polarized components that are displaced slightly in wavelength, with the observed reversal due to the tradeoff in dominance of one line wing over the other (e.g., Babcock 1947). The technique has been employed extensively in solar research, studies of magnetic main-sequence stars, and was used to search for magnetic white dwarfs to sensitivities of $\sim 1 \text{ kG}$ (Schmidt & Smith 1994; Schmidt & Grauer 1997). The instrument need only resolve the line profile, not the Zeeman splitting itself.

A magnetic field value based on a circular polarization reversal measures the mean longitudinal component of the field in the emission region, commonly termed the “effective” field strength. Using the analytical technique described by Schmidt & Smith (1994), we obtain measures of B_{eff} for the individual strong lines as entered in Table 2. Note that the dependence of field strength on λ has disappeared and because the polarization reversals are due to the mismatch between line wings, the derived values are much lower. We conclude that the mean longitudinal magnetic field strength in the funnel gas of V884 Her is $\sim 30 \text{ kG}$. Arguments presented above regarding the constancy of polarization sign in the lines suggest that orbital variations do not carry the field lines through the plane of the sky, hence that any phase dependence in field strength must be confined to the approximate range $0 \lesssim B_{\text{eff}} \lesssim 60 \text{ kG}$. Assuming radial field lines in the line-emitting portion of the funnel, this bounds $i + \delta \leq 90^\circ$, the same limit as is placed by the presence of X-rays through the entire orbital cycle (Greiner et al. 1998).

3. CLUES TO A HIGH MAGNETIC FIELD

In attempting to understand the complex spectrum of broad and narrow polarization features in V884 Her, we begin by looking to the basic properties of the system for clues to the appropriate field strength regime.

First is the correlation between X-ray flux ratio $F_{\text{SX}}/F_{\text{HX}}$ and magnetic field strength that was noted in §1 as a motivation for this study. The ratio of >1000 measured for V884 Her exceeds that on any other magnetic CV (even AR UMa only measures ~ 60 ; Szkody et al. 1999), and for reasonable extrapolations of Ramsay et al.’s (1994) correlation, suggests a polar field $B_p \gtrsim 80 \text{ MG}$.

A second indicator for a high magnetic field is our detection of Zeeman splitting in the funnel emission lines. The only previous instance where this has been observed is the $B_p = 230 \text{ MG}$ system AR UMa, where polarization reversals with a separation of up to 30 \AA were found to form curious, entwined patterns through the orbital cycle (Schmidt et al. 1999). The basic origin of that behavior is understood to be the transfer of polarized radiation in optically-thick, magnetized streamlines (Ferrario, Wickramasinghe, & Schmidt 2000). The splitting in V884 Her retains a constant sense throughout the orbit and amounts to $\sim \frac{1}{2} - \frac{2}{3}$ that in AR UMa. Assuming that the polarized line emission originates in the same portion of the funnel in both systems and that all other factors are equal, this suggests that the magnetic field on the white dwarf in

V884 Her is in the range $B_p = 100 - 150 \text{ MG}$.

A field of $100 - 150 \text{ MG}$ places the cyclotron fundamental at $\lambda = 1.1 - 0.7 \text{ \mu m}$. The optical portion of the spectrum would then sample low-harmonic cyclotron emission, $n = 1 - 3$. Based on our understanding of the lower- B AM Her systems, we would not expect this emission to be strongly beamed, so variability over the orbit will be small. This is as observed in V884 Her. Nevertheless, both the degree and variability in polarization will tend to increase with increasing harmonic number (decreasing wavelength), also as observed.

Thus, the properties of the impact region, the magnetic field strength in the accreting gas, and the cyclotron emission characteristics all point toward a high magnetic field on the white dwarf of V884 Her, $B_p \gtrsim 100 \text{ MG}$. In the following section we quantify this result through calculations of the hydrogen Zeeman spectrum and polarization with the goal of modeling the pattern of “narrow” polarization features in our data.

4. ZEEMAN-SPLIT HALO ABSORPTION LINES AT $B = 150 \text{ MG}$

In Table 3 we list the locations of the circular polarization features that are also visible in absorption and persist throughout the orbital cycle, as well as a few weaker features that appear significant in the coadded data of Figure 4. The fact that the features appear during what are clearly active accretion states argues that they should be attributed to Zeeman-split absorption in a relatively cool “halo” that overlies the bright continuum source, and not photospheric features of the white dwarf. Halo absorption was originally noted as a polarized $\text{H}\alpha$ component that was visible only during the bright phase of ST LMi (Schmidt, Stockman, & Grandi 1983), but rich patterns have now been detected in a number of systems, allowing independent measures of the magnetic field strength near the shock (e.g., Wickramasinghe, Tuohy, & Visvanathan 1987). The narrowness of the features in V884 Her, coupled with the lack of significant wavelength shift with orbital phase, is also indicative of an origin as halo Zeeman lines against a localized bright spot, as opposed to the rotation of, e.g., an oblique dipolar field pattern distributed over the surface of the star.

With the considerations of §3 as a guide, we have found that the pattern of features in V884 Her can be successfully interpreted as absorption by hydrogen in an essentially uniform magnetic field of $B = 150 \text{ MG}$. The quality of the agreement is depicted in the top panel of Figure 4, where we include the behavior of prominent components of the Balmer series for $B = 0 \rightarrow 150 \text{ MG}$, taken from calculations of Forster et al. (1984), Wunner et al. (1985), and Wunner, Geyer, & Ruder (1987). Identifications for individual spectral features are given in Table 3. Where strong signatures appear in both polarization and spectral flux – i.e. shortward of $\text{H}\alpha$ – we consider the assignments certain. The red features are more problematic, being much weaker in polarization and confused by other spectral features. For example, unpolarized line emission, like He I $\lambda 6678$ superposed on the $2p1 - 3s0$ absorption, dilutes the degree of polarization but does not directly affect polarized flux such as is displayed in Figure 4. Terrestrial absorption bands, on the other hand, reduce the observed flux level and therefore the measurement precision, but do not

modify $v(\%)$. It should be noted that the behavior shown in Figure 4 confirms our choice of a uniform-field absorbing layer, since several of the transitions (esp. the H α π components at $\lambda\lambda 5516, 5778, 5930$) are so sensitive to magnetic field strength that they would be smeared to invisibility if the spread were larger than $\Delta B \sim 10\%$. Note also that a tentative field strength estimate for V884 Her of $B_p \approx 120$ MG (Schmidt 1999) is superseded by this new measurement.

It is clear from Figure 4 that the prominent polarization features are all positive-going excursions. This includes purely σ^+ transitions like the crossing of H β components at $\lambda 4940$, as well as the H α π transitions in the range $5500 - 6000$ Å. In general, σ^- components move so rapidly with B that they are not observed in high-field situations. What is surprising is that the observed σ^+ and π components do not show detectable Doppler shifts with phase ($\Delta\lambda < \pm 20$ Å) as would be expected if these lines were formed in free-falling pre-shock material. In the lower-field systems EF Eri and V834 Cen, Doppler variations of $\Delta\lambda > \pm 50$ Å ($\Delta v > \pm 2000$ km s $^{-1}$) are observed as gas in the low-density parts of the accretion flow is heated by hard X-rays (bremsstrahlung) emanating from shocks that are formed at the base of high-density parts of the stream (Achilleos, Wickramasinghe & Wu 1992; Schwope & Beuermann 1990).

The halo lines in V884 Her appear instead to be occurring in a virtually static reversing layer. This difference may be related to the nature of the accretion shock. The various possibilities have been summarized by Wickramasinghe & Ferrario (2000). At $B = 150$ MG, the accretion shock is expected to be cyclotron-cooling dominated. The shock height h is expected to be very much less than its lateral dimension d so that the shock will be cooled from the upper surface. As a consequence, a steep temperature gradient is expected to develop in the vertical direction, just as in a stellar atmosphere. We argue below that the reversing layer that gives rise to the Balmer lines is most probably composed of nearly stationary post-shock material that is heated by the cyclotron radiation emanating from the accretion shock itself. Static reversing layers have been predicted for so-called ‘‘bombardment’’ solutions (Woelk & Beuermann 1992). However, these are unlikely to apply in the regions of high specific accretion rate that are required to provide the underlying continuum against which the Balmer lines are formed.

In order to understand the physical processes that might be occurring in the reversing layer, we first consider what we would expect from a photospheric patch with a nearly uniform field strength on the surface of a magnetic white dwarf. We set the effective temperature to $T_{\text{eff}} = 14,000$ K to ensure that the reversing layer is cool enough to produce Balmer line absorption. The mean field threading the patch is 150 MG, it has a spread in strength of ± 5 MG, and is viewed at an angle of 50° to the mean field direction. The calculations are based on the magnetic white dwarf atmosphere code developed by Wickramasinghe & Martin (1979), and include magnetobremsstrahlung opacity as in Pacholczyk (1976). Magneto-optical effects are included both in the lines and in the continuum, and for the individual broadening of the Zeeman components, as described in Wickramasinghe (1995).

Results of the calculations are shown in Figure 6. The model produces circular polarization in the π components, as observed in the data, arising from the conversion of linear polarization to circular polarization through Faraday mixing as the radiation propagates through the reversing layer. The Faraday (or magneto-optical) effects involve the continuum since they are seen in isolated π components. These results strongly support the identifications proposed in the previous section and listed in Table 3. Most of the theoretically calculated transitions appear to be represented in the data. Ignoring for the time being the broad, positive-going polarization bump centered around $\lambda 7150$, we see that the model reproduces the basic characteristics of the observed polarization spectrum: a generally negative level of circular polarization in the continuum and strong positively-directed polarization features for each of the major halo Zeeman lines. In good correspondence to the data, the π features tend toward, but do not exceed $v = 0$, while net positive circular polarization is computed for the strongest σ^+ transitions. The model shows that the positively-polarized σ^+ components that occur in the red part of the spectrum are much weaker than the components at shorter wavelengths, and indeed they are also very weak or absent altogether in the observations.

The photospheric model qualitatively explains the polarization properties of the absorption lines but fails to provide an adequate description of the observed continuum polarization. Both the narrow absorption feature predicted at 7150 Å and the associated broad polarization hump centered at this wavelength result from photospheric absorption at the cyclotron fundamental. Since a free electron gyrating in a magnetic field radiates the same sense of circular polarization as a σ^+ line component, and we are dealing with an absorption process, the predicted cyclotron feature shares the same polarization characteristics as the σ^+ components. The width of the cyclotron feature results from the field strength spread that has been allowed for in the atmosphere calculation. The cyclotron absorption feature is, however, not present in the data, and the data show a strong negative polarization hump in the wavelength region $6700 - 8000$ Å, the opposite sense to what is calculated in the model. Furthermore, there are spectral regions in the data where the polarization is essentially zero, which is again inconsistent with the photospheric model. The shortcomings of the model in regard to the continuum polarization suggest that although the reversing halo is optically thick to the Balmer lines, it is optically thin to cyclotron absorption and also to other continuum absorption processes such as bound-free absorption. Indeed, the spectral intervals with very low polarization are appropriate for continuum emission that originates from an optically-thick underlying shock and passes through the reversing layer virtually unaffected. The situation is therefore different from the photospheric model that we have presented since in the model the radiative flux at large optical depths becomes polarized as it flows through the atmosphere.

5. A CYCLOTRON ORIGIN FOR THE POLARIZATION HUMPS

At $B_p = 150$ MG, the cyclotron fundamental lies at 7150 Å. The existence of the broad polarization hump around this wavelength cannot be coincidental, and we

identify it with emission at the fundamental. Because it is in emission, the polarization has the opposite sign to that of the positively-polarized σ^+ absorption features. In addition, it appears asymmetric in polarized flux (Figure 4), with a tail extending to long wavelengths. Red wings to cyclotron emission features result from the high-energy tail of the relativistic Maxwellian electron velocity distribution (e.g., Wickramasinghe & Ferrario 2000). The first cyclotron harmonic ($n = 2$) would then be located off the blue end of our spectrum near 3600 \AA , and we identify both the gently increasing (negative) polarized flux as well as the rise in total spectral flux as one moves shortward of 6000 \AA as the red tail of this peak. In isolation, the tail would presumably increase smoothly in strength and connect with the strong negatively-polarized segment in the region $4050 - 4200 \text{ \AA}$.

The polarization reversal between 4200 \AA and 5000 \AA could in principle be a cyclotron feature from a second accretion pole of opposite polarity, but the absence of another positively-polarized harmonic in the observed spectral region would require that this be the fundamental, implying a field strength at the second pole of $\sim 240 \text{ MG}$. Moreover, the fact that both this hump and the 7150 \AA feature are present throughout the entire orbit would require both poles to be on our hemisphere continuously, an unlikely configuration for standard dipolar field geometries. Instead, we point out the confluence of Zeeman halo components from $H\gamma$ and $H\beta$ that fall in the region $\lambda = 4000 - 5000 \text{ \AA}$, only the strongest of which are indicated in Figure 4. As we have seen, all of the π and σ^+ transitions yield positive features in circular polarization, and taken together could produce the structured hump in this region. The Zeeman features are seen against the beamed higher-harmonic cyclotron emission, which is more sensitive to viewing angle than the 7150 \AA fundamental, and we attribute the phase dependence of polarized flux in the $4000 - 5000 \text{ \AA}$ region (Figure 2) to variable cancellation as the white dwarf rotates. As a consistency check on this explanation, we note from Figures 2 and 3 that when the cyclotron features (filled circles and filled squares in Figure 3) are strongest, $0.4 \lesssim \varphi \lesssim 0.8$, the $4000 - 4250 \text{ \AA}$ peak (open circles) is strongly negative and the positive hump (open triangles) is relatively weak. The converse is true when the cyclotron features are comparatively weak ($0.0 \lesssim \varphi \lesssim 0.2$).

Within the context of the modern model of profiled accretion shocks in AM Her variables (e.g., Schmidt, Stockman & Grandi 1986; Wickramasinghe & Ferrario 1988; Wu & Chanmugam 1988), the low-harmonic cyclotron emission from V884 Her presumably arises in a low- m tail of very low optical depth ($\Lambda \lesssim 100$ to provide the observed polarized emission within the harmonic) and comparatively large area. In attempting to model this region, we note that the polarization of the Zeeman lines constrains the angle between the line of sight through the halo and the field direction to be in the range $0^\circ \lesssim \theta \lesssim 60^\circ$ over the orbit. The lack of movement with phase of the 7150 \AA cyclotron feature places additional restrictions on the range in B and θ for the region producing the low-harmonic emission. Of course, these constraints must be consistent with limitations on i and δ derived from our emission line spectropolarimetry (§2.2) and the light curve at higher energies

(e.g., Greiner et al. 1998; Hastings et al. 1999).

The simplest of models used to calculate cyclotron spectra are constant- Λ models (Wickramasinghe and Meggitt 1985) that assume uniform conditions within the shock but allow for optical depth effects. The emergent intensity and polarization along a given pathlength are calculated as a function of viewing angle θ , electron temperature T_e , harmonic number n , and optical depth parameter Λ . We show in Figure 4 a series of polarization spectra from models that have been constructed with $T_e = 5 \text{ keV}$ and $\Lambda = 20$. The choice of T_e is arbitrary, but the unusually low value for Λ ensures that the cyclotron fundamental is marginally optically thick and polarized. The sequence corresponds to viewing angles $\theta = 20^\circ, 30^\circ, 40^\circ, 50^\circ$ relative to the field direction and field strengths $B = 115, 120, 125, 130 \text{ MG}$ respectively. In each case, the field has been chosen so that the broad polarization feature centered at 7150 \AA corresponds to the cyclotron fundamental. The calculations show that it should be possible to obtain qualitative agreement with the observations using a structured shock model that encompasses a spread in field strength and direction. For example, the 50° model exhibits a large excursion to negative polarization around 4000 \AA , very similar to the observations during the $\varphi = 0.4 - 1.0$ interval (Figure 2). Conversely, the model for $\theta = 20^\circ$ shows only a weak $n = 2$ harmonic feature, and the polarized flux would be dominated for $\lambda \lesssim 5000$ by the positively polarized Zeeman lines, resembling the data for the $\varphi = 0.0 - 0.2$ period. A small viewing angle with respect to the field at this time is in agreement with the presence of an X-ray eclipse due to funnel material that defines $\varphi = 0$.

These models are, however, by no means unique. For the calculations presented, the change in polarized flux between the first harmonic and the fundamental is due purely to a change in viewing angle. The polarized flux ratio is also sensitive to Λ , and in a true structured shock the two variables are unlikely to be independent. A different choice for T_e would also result in a similar series of model fits, but with a different value of Λ . Indeed, the frequency of a given cyclotron harmonic – and therefore the derived field strength – depends on B , T_e , and θ . For the 5 keV models, the disparity between the Zeeman field of 150 MG , and the cyclotron field of $115 - 130 \text{ MG}$, is significant. Lower electron temperatures would bring the two values into better agreement, but it is then difficult to obtain significant polarized flux at the first harmonic ($n = 2$). A higher viewing angle would also decrease the discrepancy, but this would imply that the field direction in the cyclotron region is significantly different from that of the halo. For a centered dipole, the disparity between the halo Zeeman and cyclotron field strengths implies an unlikely large geometrical extent to the shock region ($\Delta\delta \sim 40^\circ$). Again, this can be reduced if one adopts a more complex field structure. A dipole offset along its axis toward the observer increases the field gradient along the stellar surface, decreasing the corresponding length of the accretion arc.

Of course, the actual observed degree of polarization at any wavelength depends on the importance of competing sources of light. Between emission harmonics, the accretion tail is optically thin and the light output is presumably dominated by the optically thick, and thus unpolar-

ized, Rayleigh-Jeans emission from interior shock regions that have the traditionally large values of Λ ($\sim 10^4 - 10^6$). This region of the flow is what produces the strongly polarized and often well-defined cyclotron emission peaks in the higher harmonics ($m \sim 5 - 10$) that are observed in the optical from primary stars with lower field strengths. In V884 Her, the corresponding spectral region lies in the UV. Because the net polarization within the low- \dot{m} cyclotron emission features only reaches $v \sim 5 - 10\%$, and the harmonic emission itself is likely strongly polarized, the low- \dot{m} , low- Λ tail may provide as little as 10% of the light at those wavelengths.

In closing this section, we note that a variety of alternative interpretations of the polarization spectrum were considered, using traditional high- Λ shocks. These semi-quantitative models attempted to account for the low-polarization spectral regions by assigning them to cyclotron emission harmonics, while the strongly polarized intervals were imagined to lie between harmonics. The field strength in the cyclotron-emitting region would then be ~ 175 MG. However, it was not possible to reproduce the polarization reversal and variability below 5000 Å without appealing to gross temperature and/or field structure in the shock or to the appearance of a second accretion pole of opposite polarity that is always in the visible hemisphere (as in a quadrupolar field structure). For the sake of simplicity and self-consistency, we prefer an explanation in terms of low- Λ emission harmonics. With this insight, we are now able to successfully interpret the polarization spectrum of the highest-field magnetic CV AR UMa (Ferrario et al. 2000).

6. CONCLUSIONS

As the only second AM Her variable with $B_p > 100$ MG, V884 Her displays yet another dimension to the phenomenon of magnetic accretion. In contrast to AR UMa, whose accretion duty-cycle has been $< 25\%$ since it was first observed optically in 1991 (Schmidt et al. 1999), V884 Her has never been detected in a state of inactivity. Our spectropolarimetry in a comparatively low state, some 2 mag below historical maximum light, reveals a spectrum still dominated by polarized cyclotron emission and a brilliant array of emission lines from the accretion funnel. The contrast in properties between the two systems casts further doubt on the magnetic field having any significant effect on mass loss from the companion star (see also Schmidt et al. 1999); instead we conclude that the accretion rate is more likely driven by processes which vary considerably from one object to the next and/or that are highly variable on timescales of at least a decade.

Though not recognizable in total flux spectra, Zeeman splitting in the emission lines has now been detected through circular spectropolarimetry in both systems with $B > 100$ MG, providing a potential means of identifying high-field AM Her variables where direct identification of photospheric or halo absorption features is not possible. Field strengths measured from these magnetic splittings confirm model results (Ferrario & Wehrse 1999) indicating that the bulk of the observed line emission in AM Her systems arises $\sim 10 R_{\text{wd}}$ from the surface, where the product of the funnel surface brightness and projected area is a maximum.

Less quantitative but possibly more useful as a hallmark

of a high magnetic field is the relation between soft X-ray excess and magnetic field strength. Though variables such as accretion rate and blob spectrum undoubtedly play roles, the values of $F_{\text{SX}}/F_{\text{HX}}$ measured for AR UMa and V884 Her count among the highest ratios measured for AM Her binaries. These two systems provide strong confirmation of the expected reduction in standoff height with increasing field strength, leading to eventual burying of the shock. For AR UMa, the resulting quenching of cyclotron emission appears to be complete in the optical; for the somewhat lower-field system V884 Her, the circular polarization is weak around the fundamental but increases with decreasing wavelength.

In V884 Her, we have for the first time observed the cyclotron fundamental from a magnetic white dwarf. This came through the measurement of circular polarization, not total flux, and the polarized emission appears to originate in a low- \dot{m} tail of the impact region. This tail presumably represents the first or last (or both!) gas to be stripped from the ballistic stream, a characteristic that may contribute to the apparent discrepancy in field strengths derived from the low emission harmonics *vs.* the halo Zeeman lines. Optical depth effects in this low- Λ portion of the shock may also play a strong role. We expect emission at the fundamental to be common among AM Her systems, where it is accessible. The $B_p = 92$ MG RX J1007.5–2016 (Reinsch et al. 1999) is an excellent prospect, in view of the fact that the $n = 2$ and 3 harmonics are prominent in spectral flux. Proper interpretation of these features poses new challenges for understanding the physical properties of cyclotron-cooled accretion shocks, an area not yet explored fully in astrophysics. Calculations of the type presented by Woelk & Beuermann (1996) need to be extended to the high-field regime, allowing in addition for 3-D shock structure.

G.D.S. is grateful for the hospitality and support of the Australian National University and Mount Stromlo Observatory, where this project was completed during a sabbatical leave. Studies of magnetic stars and stellar systems at Steward Observatory are supported by NSF grant AST 97-30792.

REFERENCES

- Achilleos, N., Wickramasinghe, D.T., & Wu, K. 1992, MNRAS, 256, 80
- Babcock, H. 1947, ApJ, 105, 105
- Ferrario, L., & Wehrse, R. 1999, MNRAS, 310, 189
- Ferrario, L., Wickramasinghe, D.T., & Schmidt, G.D. 2000, in preparation
- Forster, H., Strupat, W., Rosner, W., Wunner, G., Ruder, H., & Herold, H. 1984, J. Phys. B, 17, 1301
- Greiner, J., Remillard, R.A., & Motch, C. 1998, A&A, 336, 191
- Hastings, N.C., Szkody, P., Hoard, D.W., Fried, R., Vanmunster, T., Pray, D., & Kowalski, R.A. 1999, PASP, 111, 177
- Ishida, M., Greiner, J., Remillard, R.A., & Motch, C. 1998, A&A, 336, 200
- Pacholczyk, A.G. 1976, Radio Galaxies, (Oxford: Pergamon)
- Ramsay, G., Mason, K.O., Cropper, M., Watson, M., & Clayton, K.L. 1994, MNRAS, 270, 692
- Reinsch, K., Burwitz, V., Beuermann, K., & Thomas, H.-C. 1999, in ASP Conf. Proc. 157, Annapolis Workshop on Magnetic Cataclysmic Variables, ed. C. Hellier & K. Mukai (San Francisco: ASP), 187
- Schmidt, G.D. 1999, in ASP Conf. Proc. 157, Annapolis Workshop on Magnetic Cataclysmic Variables, ed. C. Hellier & K. Mukai (San Francisco: ASP), 207
- Schmidt, G.D., & Grauer, A.D. 1997, ApJ, 488, 827
- Schmidt, G.D., Hoard, D.W., Szkody, P., Melia, F., Honeycutt, R.K., & Wagner, R.M. 1999, ApJ, 525, 407
- Schmidt, G.D., & Smith, P.S. 1994, ApJ, 423, L63
- Schmidt, G.D., Stockman, H.S., & Grandi, S.A. 1983, ApJ, 271, 735
- _____. 1986, ApJ, 300, 804
- Schmidt, G.D., Stockman, H.S., & Smith, P.S. 1992, ApJ, 398, L57
- Schmidt, G.D., Szkody, P., Smith, P.S., Silber, A., Tovmassian, G., Hoard, D.W., Gänsicke, B.T., & de Martino, D. 1996, ApJ, 473, 483
- Schwope, A.D., & Beuermann, K. 1990, A&A, 238, 173
- Stockman, H.S. 1988, in Polarized Radiation of Circumstellar Origin, ed. Coyne, G.V. et al., (Vatican: Vatican Observatory), 237
- Szkody, P., Silber, A., Hoard, D.W., Fierce, E., Singh, K.P., Barrett, P., Schlegel, E., & Pirolo, V. 1995, ApJ, 455, L43
- Szkody, P., Vennes, S., Wagner, R.M., & Hastings, C. 1999, in ASP Conf. Proc. 157, Annapolis Workshop on Magnetic Cataclysmic Variables, ed. C. Hellier & K. Mukai (San Francisco: ASP), 195
- Wickramasinghe, D.T. 1995, in ASP Conf. Ser. 78, Astrophysical Applications of Powerful Data Bases, ed. Aldeman, S.J., & Wiese, W.L., (San Francisco: ASP), 319
- Wickramasinghe, D.T., & Ferrario, L. 1988, ApJ, 334, 412
- _____. 2000, PASP, 112, 873
- Wickramasinghe, D.T., & Martin, B. 1979, MNRAS, 188, 165
- Wickramasinghe, D.T., Tuohy, I.R., & Visvanathan, N. 1987, ApJ, 318, 326
- Woelk, U., & Beuermann, K. 1992, A&A, 256, 498
- Woelk, U., & Beuermann, K. 1996, A&A, 306, 232
- Wu, K., & Channugam, G. 1988, ApJ, 331, 861
- Wunner, G., Geyer, F., & Ruder, H. 1987, Ap&SS, 131, 595
- Wunner, G., Rosner, W., Herold, H., & Ruder, H. 1985, A&A, 149, 102

TABLE 1
LOG OF OBSERVATIONS

UT Date (yyyymmdd.dddd)	φ	Type	m_V (mag)	Polarization
19980522.4616-.4689	0.60–0.69	Cir. Spectropol.	16.1	–1.83%
19980923.1077-.2060	0.07–1.32	Cir. Spectropol.	16.2–16.6 ^a	–1.32 to +0.57%
19990518.3515-.4376	0.11–1.25	Cir. Spectropol.	16.0–16.3 ^a	–1.20 to +0.14%
19990914.1599-.2476	0.94–1.06	Lin. Filter Pol.	...	$0.30 \pm 0.11\%$ @ 164°
19991014.1495-.1568	0.05–0.14	Spectroscopy	15.3	...
20000310.4264-.4796	0.42–1.10	Cir. Spectropol.	15.7–15.9	–1.00 to –0.75%

^aIntermittent light clouds

TABLE 2
ZEEMAN SPLITTING IN THE EMISSION LINES

Feature	B_{eff} (kG)
H α	25
H β	32
He II λ 4686	35
H γ	20
H δ	21

TABLE 3
POLARIZED HALO LINES OF HYDROGEN

λ (Å)	Identification ($B=150$ MG)
4296	2p–1 – 3d0 (σ^-), 2s0 – 4f0 (π), 2p1 – 5s0 (σ^+)
4480	2p0 – 3s0 (π), 2p0 – 4d–1 (σ^+), 2p1 – 5d0 (σ^+)
4940	2s0 – 4f–1 (σ^+), 2p1 – 4s0 (σ^+)
5516	2p–1 – 3d–1 (π)
5778	2p0 – 3d0 (π)
5930	2s0 – 3p0 (π)
6645,6690 (?)	2p1 – 3s0 (σ^+)
6847 (?)	2s0 – 3p–1 (σ^+)

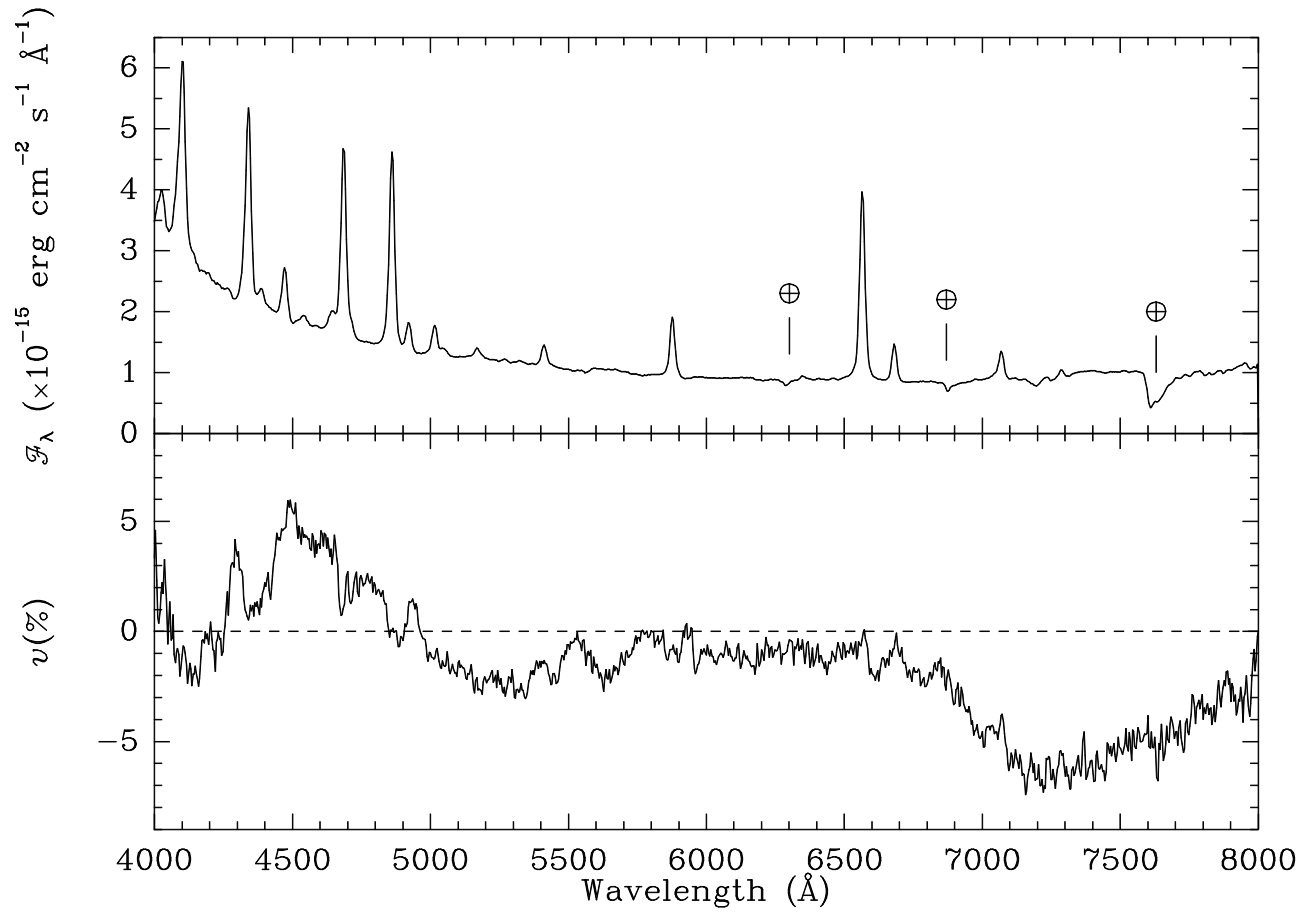


FIG. 1.— Orbit-averaged total flux and circular polarization spectra of V884 Her from 1998 Sep. 14. Note the comparatively weak level of circular polarization for a magnetic CV and the highly structured appearance, particularly for $\lambda < 5000$ Å. Terrestrial absorption features affecting the spectral flux are noted.

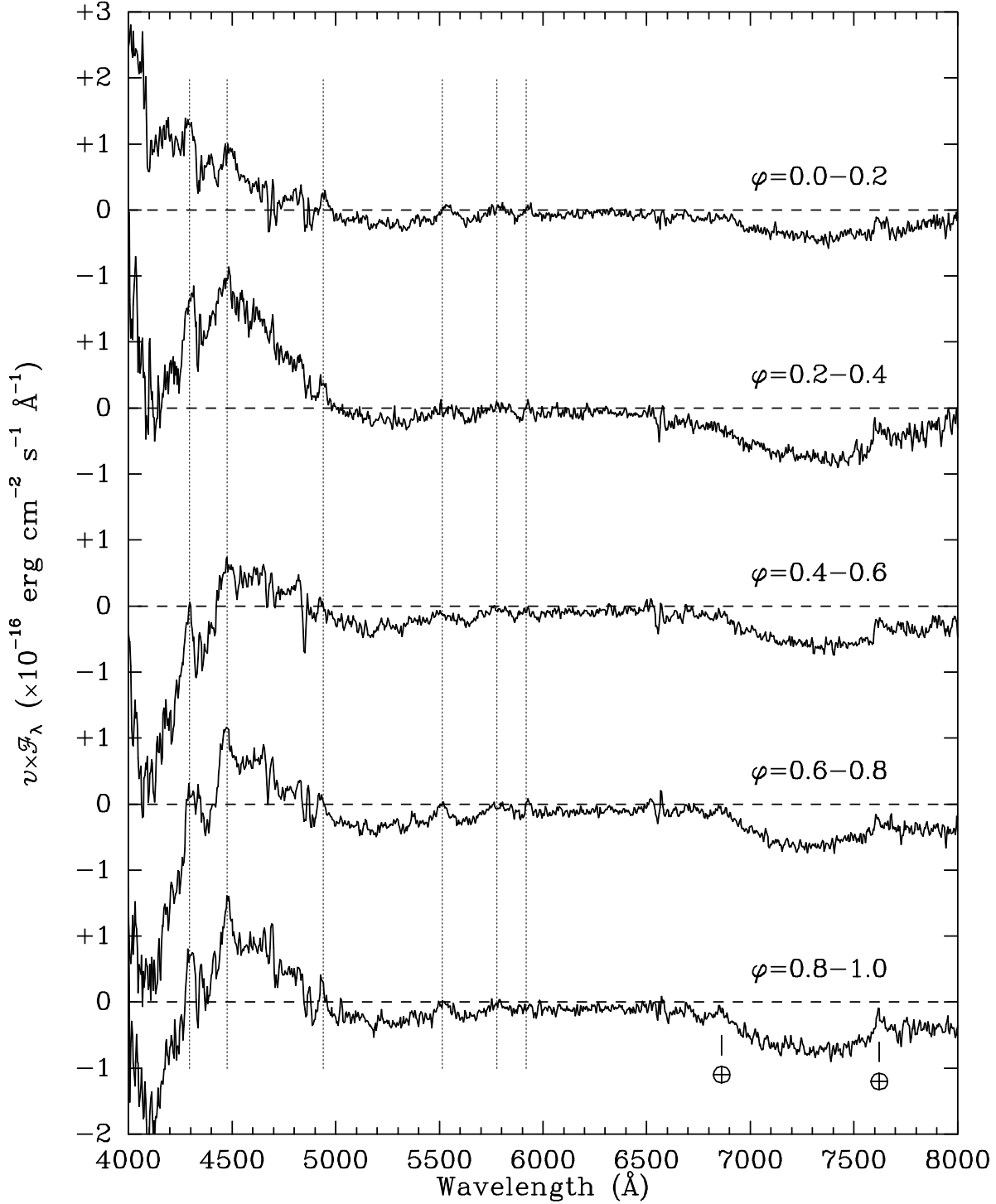


FIG. 2.— Phase-binned circularly polarized flux of V884 Her averaged over all 3 epochs and with the orbital motion removed. Variability is confined largely to the bluest wavelengths. Sharp polarization reversals in each of the major emission lines $\text{H}\alpha$, $\text{H}\beta$, $\text{He II } \lambda 4686$, etc. signify Zeeman splitting in the funnel. Several narrow polarization features that remain nearly stationary with phase are indicated by dotted lines.

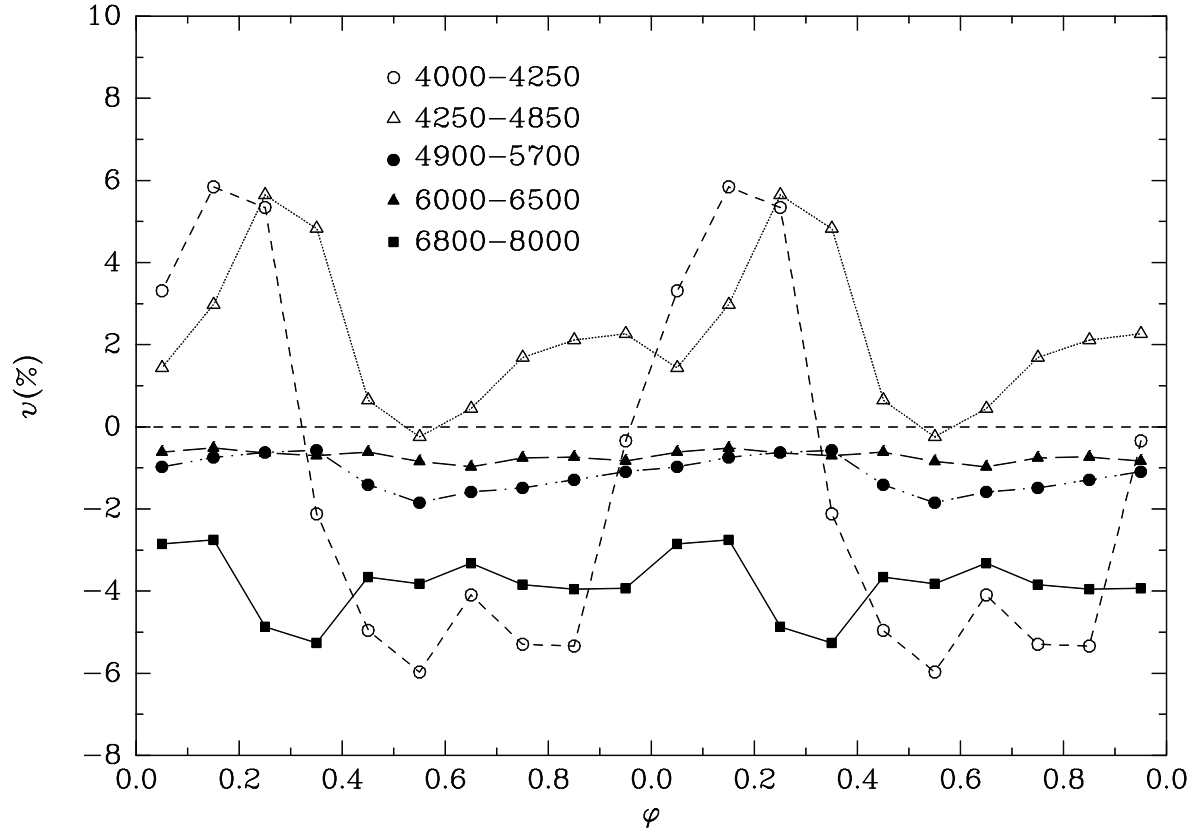


FIG. 3.— The phase dependence of circular polarization in broad spectral bands chosen to isolate major features. Note the small and relatively constant level of polarization in the red.

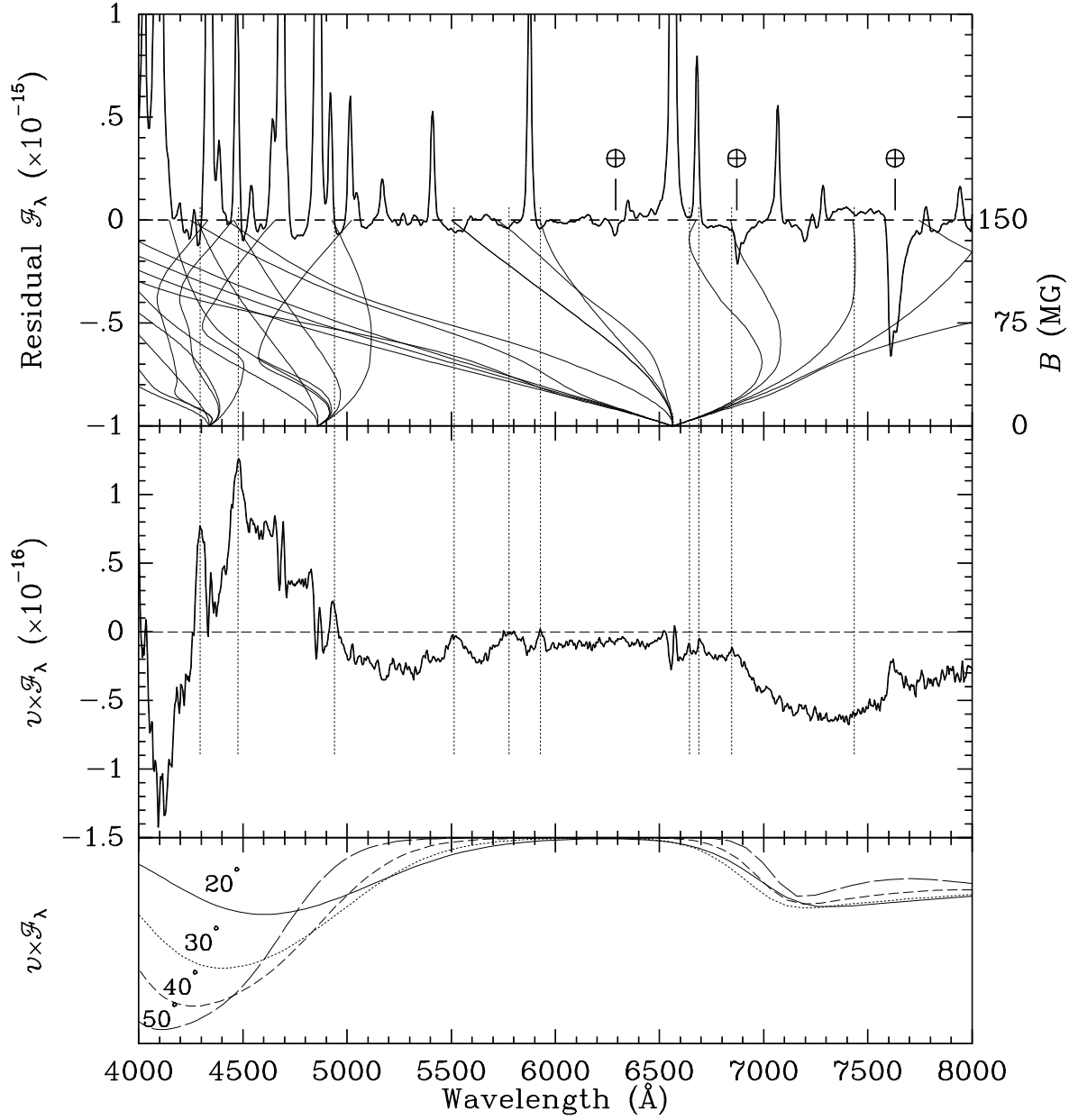


FIG. 4.— *Top*: Total flux spectrum of V884 Her after subtraction of a low-order polynomial fit to the continuum. Smooth lines depict the magnetic field dependence of the principal lines of hydrogen for $B = 0 \rightarrow 150$ MG. *Middle*: Circularly polarized flux coadded over all orbital phases and epochs. With orbital motion removed, sharp polarization reversals are evident across each major emission line, a result of Zeeman splitting within the funnel. Several positive-going polarization features – indicated by dotted lines – are accompanied by weak absorption dips in the total flux, and match the locations of strong hydrogen transitions for $B = 150$ MG. *Bottom*: Model results for constant- Λ , $T_e = 5$ keV shocks for the indicated values of θ from the field direction. In order to fix the cyclotron fundamental at its observed wavelength around 7150 Å, the field strength varies over $B = 115, 120, 125, 130$ MG for the $\theta = 20^\circ, 30^\circ, 40^\circ, 50^\circ$ curves, respectively.

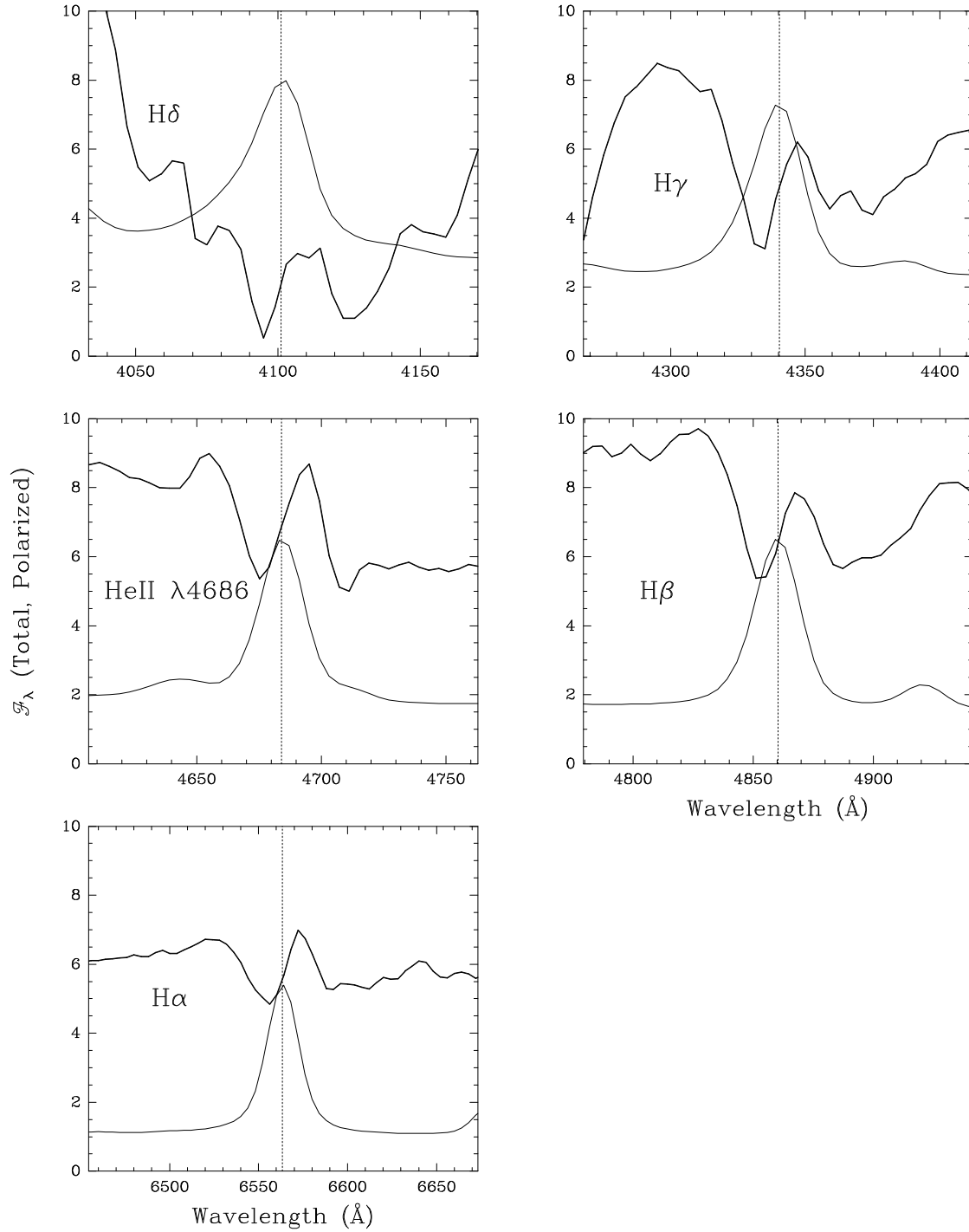


FIG. 5.— Circularly polarized flux (*bold*) and total flux (*thin*) of principal emission lines in V884 Her showing Zeeman splitting of the funnel gas in a longitudinal magnetic field of strength $B_{\text{eff}} \approx 30$ kG.

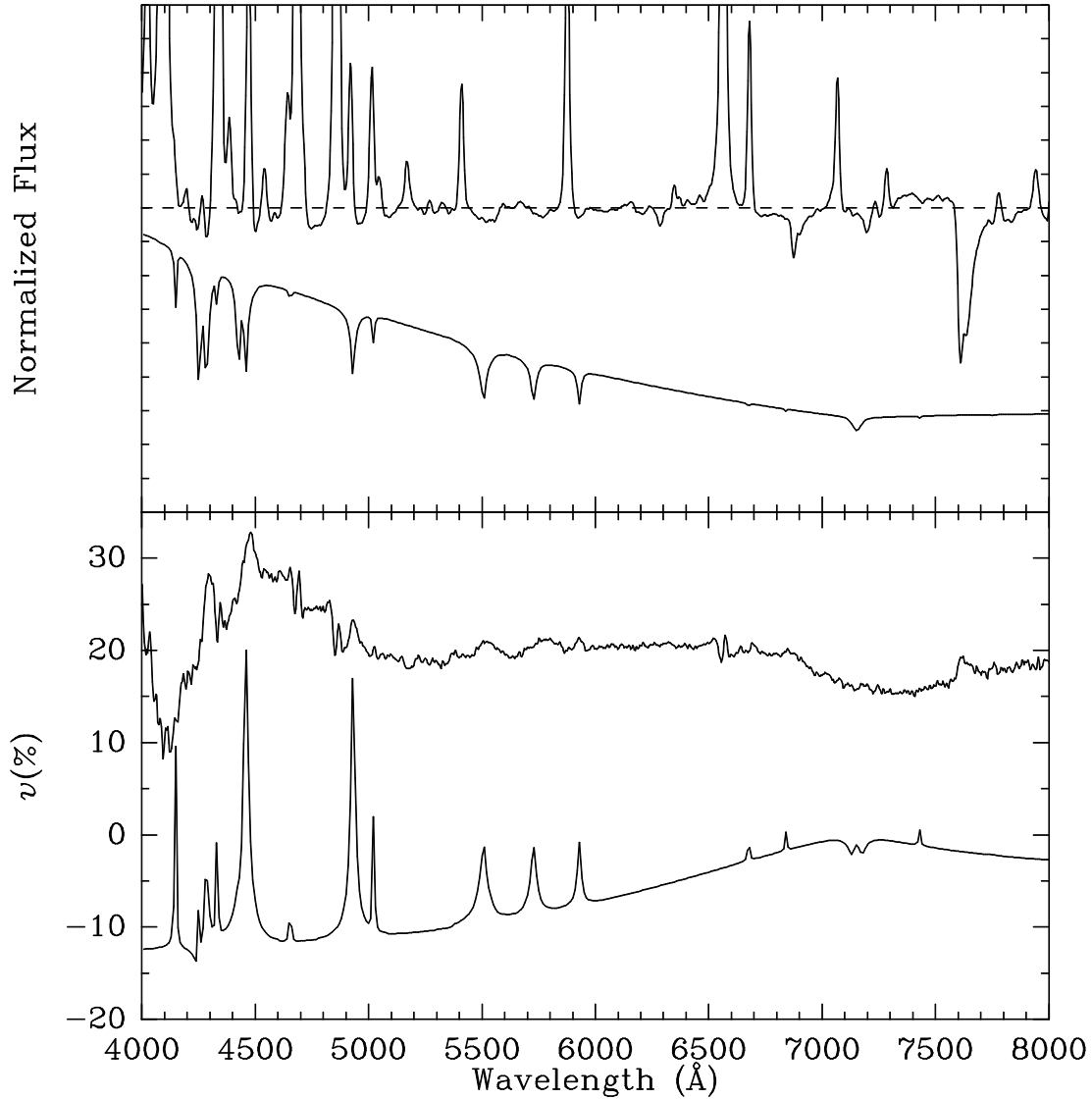


FIG. 6.— Calculated total flux (*top panel*) and circular polarization (*bottom panel*) spectra for a photosphere threaded by a uniform magnetic field of $B = 150$ MG and viewed from an angle of 50° to the field direction. Note the weakness of features in the red and the appearance of the π absorption features between 5500 and 6000 Å in circular polarization, a result of magneto-optical (Faraday) effects. The broad hump centered around $\lambda 7150$ is the cyclotron fundamental. The model curves are compared with the observed residual flux and circularly polarized flux from Figure 4, displaced for clarity.